NANO LETTERS
Letter
Cite This: Nano Lett. 2018, 18, 2816−2821
pubs.acs.org/NanoLett

Resolving the Chemically Discrete Structure of Synthetic Borophene Polymorphs

Gavin P. Campbell,[†,#] Andrew J. Mannix,[†,‡,#] Jonathan D. Emery,[†] Tien-Lin Lee,[§] Nathan P. Guisinger,[‡] Mark C. Hersam,[†,∥] and Michael J. Bedzyk*[,†,⊥]

[†]Department of Materials Science and Engineering, [∥]Department of Chemistry, and [⊥]Department of Physics and Astronomy, Northwestern University, Evanston, Illinois 60208, United States

[‡]Center for Nanoscale Materials, Argonne National Laboratory, Argonne, Illinois 60439, United States

[§]Diamond Light Source, Harwell Science and Innovation Campus, Didcot OX11 0DE, United Kingdom

Supporting Information

ABSTRACT: Atomically thin two-dimensional (2D) materials exhibit superlative properties dictated by their intralayer atomic structure, which is typically derived from a limited number of thermodynamically stable bulk layered crystals (e.g., graphene from graphite). The growth of entirely synthetic 2D crystals, those with no corresponding bulk allotrope, would circumvent this dependence upon bulk thermodynamics and substantially expand the phase space available for structure−property engineering of 2D materials. However, it remains unclear if synthetic 2D materials can exist as structurally and chemically distinct layers anchored by van der Waals (vdW) forces, as opposed to strongly bound adlayers. Here, we show that atomically thin sheets of boron (i.e., borophene) grown on the Ag(111) surface exhibit a vdW-like structure without a corresponding bulk allotrope. Using X-ray standing wave-excited X-ray photoelectron spectroscopy, the positions of boron in multiple chemical states are resolved with sub-angström spatial resolution, revealing that the borophene forms a single planar layer that is 2.4 Å above the unreconstructed Ag surface. Moreover, our results reveal that multiple borophene phases exhibit these characteristics, denoting a unique form of polymorphism consistent with recent predictions. This observation of synthetic borophene as chemically discrete from the growth substrate suggests that it is possible to engineer a much wider variety of 2D materials than those accessible through bulk layered crystal structures.

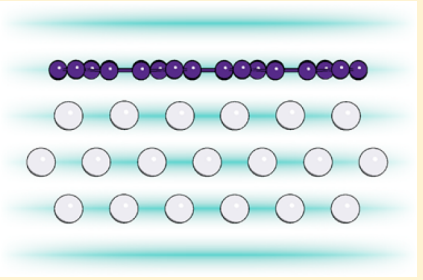

KEYWORDS: *X-ray standing wave, X-ray photoelectron spectroscopy, boron, borophene, two-dimensional materials*

Boron can form highly coordinated networks built around a motif of unconventional covalent bonds, which are frequently delocalized about three or more atoms.[1,2] Recently, two-dimensional (2D) sheets of borophene have been synthesized by depositing pure boron on atomically flat Ag(111) substrates under ultrahigh vacuum (UHV) conditions,[3,4] as illustrated in Figure 1a.

These structures are distinct from conventional atomically thin two-dimensional (2D) materials, which are derived from thermodynamically stable bulk layered crystals[5] (e.g., graphene from graphite) and exhibit superlative properties[6−8] dictated by their intralayer atomic structure. In contrast, borophene is believed to exhibit a planar form similar to laterally fused nanoscale boron clusters,[2,9−12] with a number of predicted, energetically similar vacancy superlattices characterized by a vacancy concentration ν_x.[13,14] Specifically, the β_{12} ($\nu_{1/6}$) and χ_3 ($\nu_{1/5}$) structure models, shown in Figure 1b,c respectively, have been proposed for borophene on the Ag(111) surface.[4,10,15] These structures should exhibit distinct chemical signatures due to the differences in B−B coordination numbers (labeled in the inset models), with the β_{12} structure demonstrating a 2:2:1 ratio of 4-fold, 5-fold, and 6-fold coordination and the χ_3 showing a 1:1 ratio of 4-fold and 5-fold coordination. Despite the differences in in-plane structure between the two models, the predicted vertical separation from the Ag(111) substrate is 2.4 Å in both cases, a value similar to the gap between graphene[16−18] or hexagonal boron nitride[19,20] and metal growth substrates. Because the out-of-plane structure of borophene with respect to the underlying Ag(111) substrate has not been directly quantified, it remains experimentally unclear whether borophene is comprised of boron sheets bound in a planar[4,10,15] or buckled[3] morphology or is a strongly chemisorbed adlayer. Here, we characterize the structure of borophene under pristine UHV conditions with X-ray standing wave (XSW)-excited X-ray photoelectron spectroscopy (XPS),[21,22] which measures the distribution of atoms relative to the substrate lattice with both sub-Å spatial resolution and chemical state specificity. Independent of the specific in-plane structure, borophene is found to exist as a single, atomically flat layer (i.e., minimally buckled) that is separated from the

Received: December 8, 2017
Revised: April 9, 2018
Published: April 13, 2018

DOI: 10.1021/acs.nanolett.7b05178
Nano Lett. 2018, 18, 2816−2821

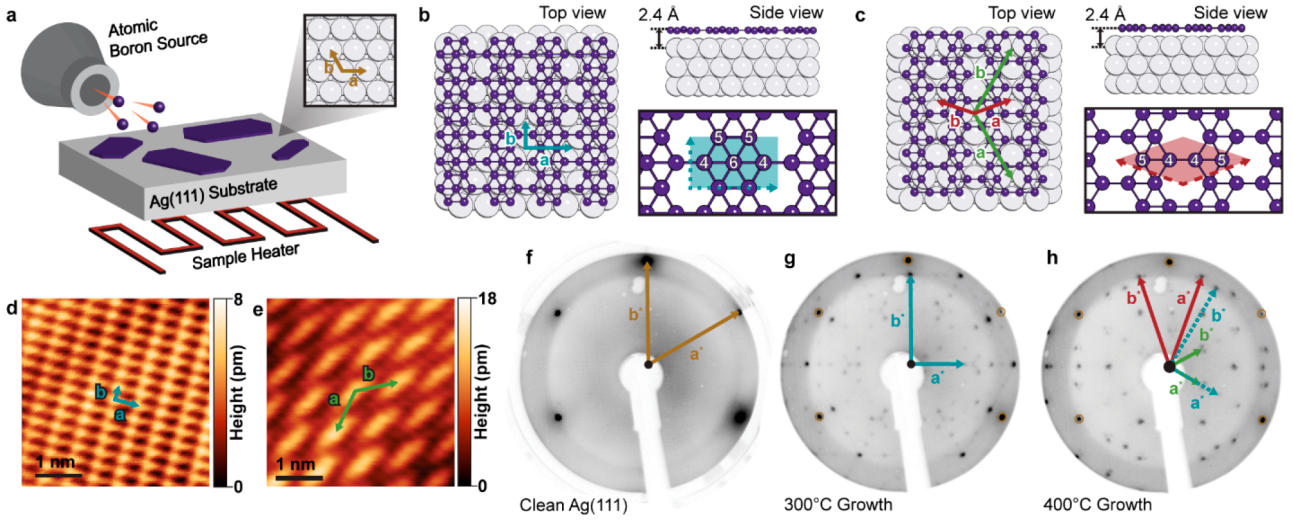

Figure 1. Borophene synthesis and atomic structures. (a) Schematic of borophene growth. (b,c) Atomic models of Ag(111)-supported borophene in the β_{12} and χ_3 structures, respectively. The enlarged models show the LEED derived rectangular (R) and diamond (D) 2D unit cells over each phase with the boron atomic coordination numbers labeled. (d,e) STM topography images showing the atomic-scale structures corresponding to the R and D phases. (f–h) LEED patterns acquired at 70 eV, corresponding to (f) clean Ag(111), (g) borophene growth at 300 °C (predominantly R phase), and (h) borophene growth at 400 °C (predominantly D phase).

underlying Ag(111) substrate by a gap of 2.4 Å with no evident B–Ag primary bonding site. This work thus experimentally demonstrates that borophene is a synthetic, elemental 2D material with no known bulk analogue.

Two structural phases of borophene have been observed experimentally via scanning tunneling microscopy (STM) and low-energy electron diffraction (LEED): a primitive rectangular phase [R phase; (Figure 1d)] and a diamond phase [D phase; (Figure 1e)],[3,4] which are expected to match the computationally predicted β_{12} and χ_3 structures, respectively.[4,15,23,24] The phase of borophene is determined by the boron deposition rate and the Ag(111) substrate temperature during growth.[3,4]

Samples of both principally R phase and D phase were grown at 300 and 400 °C, respectively, in a dedicated preparation chamber attached to the main X-ray analysis chamber at beamline I09 at the Diamond Light Source under ultrahigh vacuum (UHV, $P < 5 \times 10^{-10}$ mbar). Boron was deposited at 0.002 Å/s for 20 min to a coverage of nominally 0.3 B/Å^2, where one complete monolayer of borophene corresponds to 0.35 B/Å^2 and 0.29 B/Å^2 in the β_{12} and χ_3 models, respectively, as shown in Figure 1b,c. See Supporting Information for addition details on sample preparation.

LEED patterns were acquired to verify the 2D crystal phases present after boron deposition. The LEED pattern for the 300 °C growth (Figure 1g) is consistent with the R phase[25] and the β_{12} reciprocal lattice vectors (but rotated 30° with respect to the Ag spots). Growth at 400 °C results in a LEED pattern (Figure 1h) consistent with predominantly D phase,[3] which can be explained by a combination of the reciprocal lattice vectors of both the χ_3 and β_{12} models. See Figure S1 in Supporting Information for further discussion of the LEED patterns. As will be shown later by XPS, the 300 °C borophene is ~90% R phase and the 400 °C borophene is ~90% D phase.

Comparative STM imaging (Figure 1d,e) was performed in a separate UHV system on samples grown under similar conditions (at a growth temperature of ~400 °C), resulting in the presence of both R and D phase islands. The STM images were acquired by an Omicron-Scienta Cryo-SPM microscope at 2.5 K in constant-current topography mode, using an electrochemically etched tungsten tip.

To analyze the character of the bonds at the B/Ag(111) interface, we probed the chemical identity of the R and D phases *in situ* using XPS and XSW at the Diamond Light Source I09 beamline, which can provide both soft (100–2100 eV) and hard X-rays (2.1–20 keV) at the same spot on the sample from two separate undulators. Soft X-rays used a defocused beam size of 300 × 300 μm^2. Hard X-rays were focused down to 40% of the original 300 × 300 μm^2 beam size. XSW measurements were acquired using hard X-rays in a back-reflection geometry (i.e., $\theta_B \lesssim 90°$) to maximize the B 1s yield and minimize the effect of Ag(111) mosaicity.[21] An incident beam energy of E = 2.629 keV was selected by tuning the first harmonic of the I09 undulator and the Si(111) double-crystal monochromator. At this energy, the incident beam fwhm bandwidth was E = 0.36 eV. We measured O 1s, Ag 3d, C 1s, B 1s, and survey XPS spectra at variable soft X-ray energies, the fwhm bandwidth was E = 90 meV at 500 eV. No evidence of other elements (namely, oxygen or carbon) was observed in the survey scans (Figure S2), verifying a chemically pure borophene sample. Borophene samples were found to tolerate X-ray irradiation with no apparent degradation (i.e., no change in B 1s signal) despite multihour X-ray exposures.

Figure 2 shows high-resolution B 1s and Ag 3d core-level spectra for borophene grown at 300 and 400 °C. In both samples, the B 1s spectra (Figure 2a) are composed of a common set of chemically shifted components and are considerably narrower than multilayer boron B 1s spectra (Figure S3). This observation suggests that the boron atoms in borophene occupy discrete local bonding environments. In bulk-derived 2D crystals, observations of multiple binding energies in the core-level spectra of the 2D material are accompanied by vertical undulations in the long-range structure[19,26–28] and deviations from intrinsic material properties.[29,30] These binding energy shifts are therefore attributed to disparate atomic interaction strength with the underlying substrate. In the case of borophene, the B 1s spectra can be fit with five individual components, which we instead attribute

DOI: 10.1021/acs.nanolett.7b05178
Nano Lett. 2018, 18, 2816–2821

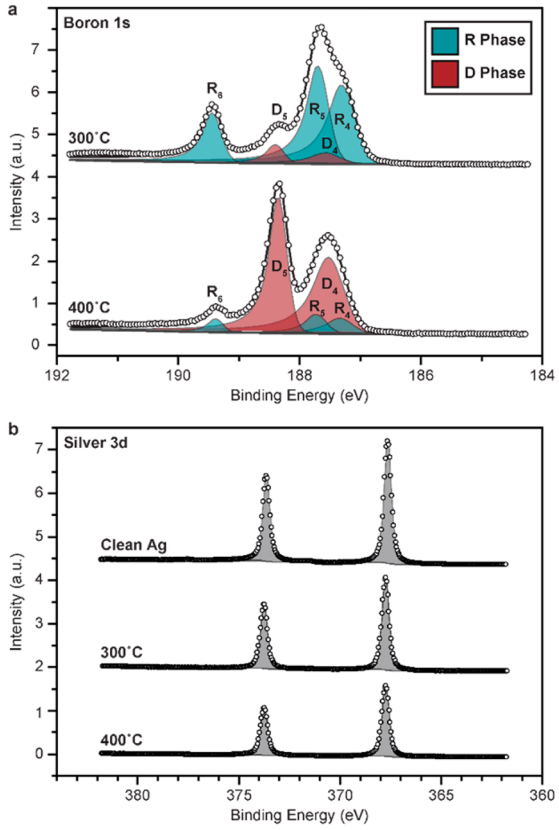

Figure 2. High-resolution XPS. (a) Boron 1s core-level spectra for borophene samples grown at 300 and 400 °C. (b) Silver 3d core-level spectra of clean Ag(111) and borophene samples grown at 300 and 400 °C. Both plots display the raw data (dots), fitted peak components (filled shapes), and fitted envelope (gray line).

to different B−B coordination numbers present in the two principal borophene phases: three for the R phase ($R_{4,5,6}$, i.e., 4-fold , 5-fold , and 6-fold coordinations) and two for the D phase ($D_{4,5}$, i.e., 4-fold and 5-fold coordinations), following the trend observed in graphene of higher binding energy corresponding to higher coordination.[31] The relative integrated peak intensity of these components reflects the proportions of boron atoms in their corresponding chemical environment. The intensity ratios show the 300 °C sample is ∼90% R phase and ∼10% D phase, whereas the 400 °C sample is ∼10% R phase and ∼90% D phase. Moreover, the ratios in peak intensities are $I_{R_4}:I_{R_5}:I_{R_6} \approx 2:2:1$ for the R phase and $I_{D_4}:I_{D_5} \approx 1:1$ for the D phase, which are consistent with the predicted ratios of 4-fold, 5-fold, and 6-fold coordinated boron atoms in the β_{12} and χ_3 borophene crystal structures.[4,10,15] In both samples, the Ag 3d spectra (Figure 2b) are indistinguishable from that of clean Ag(111), apart from mild attenuation due to the boron overlayer, which indicates the borophene samples are free of B−Ag compounds.

To investigate whether any chemical species possess a varying depth profile, we collected XPS data at 16 distinct photoemission angles.[32] Selecting a series of detector emission angles between 4° and 56° varied the effective probing depth (Λ_{eff}) for B 1s (Figure S4) and Ag $3d_{5/2}$ photoelectrons by several angströms. The relative intensity of the components of the B 1s and Ag $3d_{5/2}$ spectra shows no dependence on observed emission angle, indicating that all boron species are co-located and that the Ag(111) surface is bulk-like.

Although high-resolution XPS provides strong evidence of chemical coordination and co-location of boron species near the Ag(111) surface, precise structural determination requires spatially resolved methods. The XSW technique enhances XPS with high spatial resolution by modulating the photoelectron yield with an X-ray standing wave formed by the interference between the incident and reflected X-ray beams at the Bragg condition (Figure 3a).

The standing wave period is equal to the substrate Bragg diffraction plane *d*-spacing. Scanning the incident X-ray energy, *E*, through the Bragg condition causes the reflectivity, $R(E)$, to approach unity over an eV-wide X-ray Bragg reflection and the XSW phase, $\phi(E)$, to shift by π-radians. Chemically specific structural information is acquired by monitoring changes in XPS intensity as the standing-wave shifts from being out-of-phase with the diffraction planes to being in-phase. The resulting XPS modulation can be analyzed to find the substrate lattice location of various atomic species both above and below the crystal surface.[33,34] Such measurements have previously proven to be effective in determining the chemically precise structure of 2D material interfaces.[16,19,27] Here, we use XSW-enhanced XPS to extract ensemble-averaged vertical positions of the surface silver and the chemically distinct boron species for both R and D phase borophene.

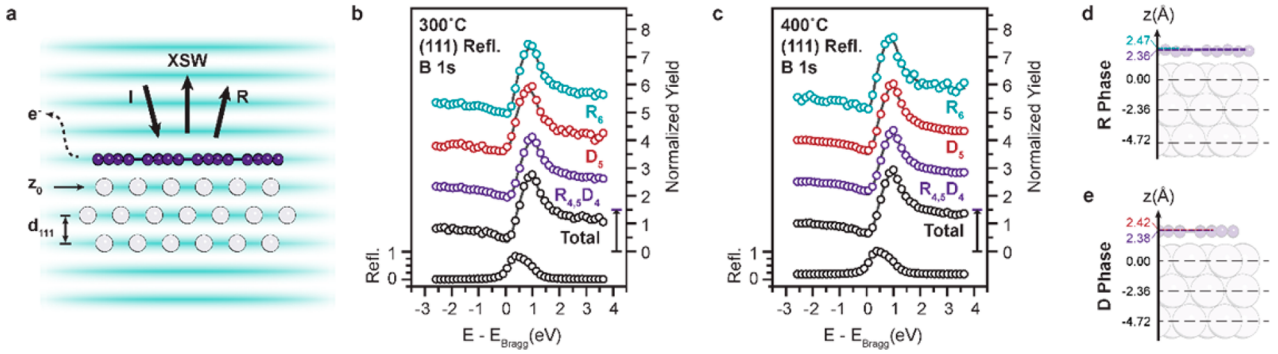

Figure 3. XSW characterization of the borophene/Ag(111) structure. (a) Schematic of XSW (blue lines) generated by interference between the incident (I) and reflected (R) X-ray beams during Bragg diffraction from a Ag(111) single crystal with a D phase borophene layer. (b,c) Data (circles) and model fits (black lines) for incident X-ray energy dependence of the X-ray reflectivity and normalized B 1s photoelectron yields of samples grown at 300 and 400 °C, respectively. Total B 1s is shown with chemically distinct boron species from Figure 2a. (d,e) Structural characterization from XSW for the R phase and D phase derived from the 300 and 400 °C sample growths, respectively, with predicted positions from Table 1 denoted by solid lines.

DOI: 10.1021/acs.nanolett.7b05178
Nano Lett. 2018, 18, 2816−2821

Table 1. For the Two Deposition Temperatures, XPS Determined Boron Percent Speciation (from Table S1), Coherent Fraction (f_s), Coherent Position (P_s), and Mean Heights ($\bar{z}$) from XSW Analysis in Figure 3

	300 °C borophene				400 °C borophene				model[a]
	B%	f_s	P_s	$\bar{z}$ (Å)[b]	B%	f_s	P_s	$\bar{z}$ (Å)[b]	$\bar{z}$ (Å)[b]
total	100	0.92(9)	0.02(1)	2.41(3)	100	0.91(9)	0.02(1)	2.40(3)	–
R_4[c]	**37.0**	0.89(8)	0.00(1)	2.36(2)	6.8	0.89(8)	0.01(1)	2.38(4)	2.37
R_5[c]	**37.0**	0.89(8)	0.00(1)	2.36(2)	6.8	0.89(8)	0.01(1)	2.38(4)	2.31
R_6	**16.5**	0.93(8)	0.04(2)	2.47(4)	3.4	0.9 (1)	0.06(4)	2.51(9)	2.44
D_4[c]	4.5	0.89(8)	0.00(1)	2.36(2)	**41.3**	0.89(8)	0.01(1)	2.38(4)	2.28
D_5	5.0	0.8(1)	0.07(3)	2.52(3)	**41.9**	0.96(9)	0.03(1)	2.42(2)	2.31

[a]B heights based on the DFT β_{12} (R) and χ_3 (D) structural models for borophene illustrated in Figure 1b,c acquired via private communication with Boris Yakobson.[10,15] [b]Values calculated using Ag(111) *d*-spacing = 2.359 Å. [c]Values held at fixed relative B% during fitting. Bold indicates majority phase.

Depending on the precise atomic distribution the photoelectron yield from a selected chemical species (s):

$$Y_s(E) = 1 + R(E) + 2\sqrt{R(E)}f_s\cos(\phi(E) - 2\pi P_s) \quad (1)$$

gives a distinct modulation versus energy that is parametrized by the Fourier amplitude (or coherent fraction, f_s) and phase (or coherent position, P_s) of the distribution profile.[21,22] Roughly speaking the coherent position is a normalized measurement of the atomic average position $\bar{z}_s$, modulo the 2.359 Å *d*-spacing of the Ag(111) diffraction plane. The coherent fraction describes the atomic distribution width normal to the diffraction planes.[35] For example, a random distribution of atoms would produce $f_s = 0$, and $f_s = 1$ indicates all atoms are precisely located at P_s. The Ag $3d_{5/2}$ XSW-XPS yield results in $f_{Ag} = 1$ and $P_{Ag} = 1$ for all samples, indicating that all silver atoms within the ∼10 Å sampling depth are unaffected by the presence of boron. In contrast to the nearly random B 1s XSW-XPS distribution ($f = \sim 0.2$) for ∼3 layers of boron deposited at 20 °C (Figure S6), the *total* B 1s XPS yield fit of both 300 and 400 °C borophene showed $f_t > 0.9$ and $P_t = 0.0$ corresponding to a narrow single-layer boron distribution (Gaussian width $\sigma_t = 0.15$ Å) positioned at 2.4 Å above the topmost Ag(111) atomic planes. Critically, this measurement indicates that, independent of the specific phase or B−B coordination, all boron atoms in borophene have strong in-plane bonds stabilized by comparatively weak interactions with the Ag(111) surface. In this context, weak interaction is defined by the lack of resolvable primary B−Ag bonding, thus indicating that the borophene layer is chemically discrete from the underlying substrate. The 2.4 Å vertical separation of borophene from the substrate is comparable to boron atoms in hBN (2.17 Å for chemisorbed boron[19] and 3.26−3.40 Å for physisorbed boron[19,26]) which are inflated by repulsive interactions between nitrogen atoms and metal substrates.[36] The f_t and P_t values measured for borophene on Ag(111) are highly consistent with the DFT calculated values,[10,15] apart from a slightly larger-than-expected distribution width ($\sigma = 0.1$ Å expected for thermal disorder) that may be due to the very minor presence of boron clusters uncorrelated with the Ag(111) lattice (see Supporting Information for additional analysis). The relatively small calculated adhesive potential of the β_{12} structure (175 meV/atom)[10] supports our observation that the interface is free of primary B−Ag bonds. This result shows that both R and D phase borophenes are essentially planar boron polymorphs stabilized by Ag(111). Although the substrate is expected to influence the growth and properties of the borophene sheet, recent reports of metallic characteristics[37] and Dirac Fermions[25,38] in borophene suggest that the electronic structure of borophene is affected by charge donation and structural perturbations of the borophene lattice from the substrate. The weak degree of B−Ag hybridization observed in these studies is consistent with our results, although further study is necessary in order to understand deviations between these measurements and the electronic structure of freestanding borophene.[39]

Coordination-specific structural information can also be extracted from the XSW data using the peak-fits obtained from high-resolution B 1s XPS (detailed fitting procedures given in the Supporting Information). A 5-component fit of the R phase and D phase to the 300 °C (Figure 3b) and 400 °C (Figure 3c) XSW-XPS data shows nearly identical photoelectron yields ($Y_{R_{4,5,6}D_{4,5}}$) for all components. Despite the distinct in-plane registry predicted between the surface silver atoms and the boron atoms in the β_{12} and χ_3 structures, the model fitting results (Table 1) reveal that all chemically distinct species of borophene are highly planar ($f > 0.8$; Gaussian width $\sigma_t < 0.3$ Å) with essentially the same 2.4 Å spacing above the terminal plane of Ag(111) atoms ($0.0 < P < 0.1$). These results are depicted schematically in Figure 3d,e for the 300 and 400 °C borophene samples relative to the β_{12} and χ_3 structures, respectively. Thus, borophene appears free of major site-specific vertical displacements ($\Delta\bar{z}_{max} \approx 0.1$ Å), in contrast to those expected for intrinsically buckled synthetic 2D materials (e.g., 0.7 Å for silicene[28] and 0.8 Å for a buckled triangular borophene lattice[3]). Additionally, in epitaxial hBN systems ∼0.6 eV B 1s core-level shifts are accompanied by corrugations of 0.6 Å on Cu(111)[26] and 1.5 Å on Ir(111),[19] whereas for borophene comparable B 1s shifts show no accompanying vertical displacement. Statistically significant vertical displacements ($\Delta\bar{z} \approx 0.1$ Å) were only for boron species with a corresponding binding energy shift of ∼2.0 eV (Table S1). Thus, confirming that distinct boron atomic coordination induces the core-level shifts in the borophene B 1s components. Thus, a planar structure with slight distortions induced by substrate interactions (e.g., variable adsorption sites, Moiré pattern, and/or strain) provides the most reasonable explanation for these observations. The lack of resolvable spectroscopic signatures for chemical Ag−B interaction in XPS in turn suggests that this subtle corrugation results from noncovalent interaction with the substrate, although determining the exact nature of this interaction likely requires a combination of theory and laterally resolved chemical information. Notably, the observed maximum displacements for both phases are comparable to the predicted values for boron on Ag,[10,15] which suggests that this slight buckling

DOI: 10.1021/acs.nanolett.7b05178
Nano Lett. 2018, 18, 2816−2821

relative to the planar freestanding case is expected due to substrate interactions.

Based on the boron 2D lattice determination by LEED, the coordination by XPS, and height by XSW, the R and D phases observed in STM[3,4] are confirmed to be distinct in-plane vacancy configurations as predicted computationally for the β_{12} and χ_3 phases.[4,10,15] This conclusion implies that borophene exhibits a unique 2D, vacancy-mediated form of structural degeneracy that is reminiscent of the complexity observed in 3D boron allotropes. This polymorphism within the borophene family further suggests that the properties of borophene and its derivatives can be systematically modified based on substrate interactions, strain, and other parameters. Overall, these results demonstrate that materials without layered bulk allotropes can be induced to form highly planar structures at the 2D limit stabilized by comparatively weak interactions with metal substrates, thereby establishing a new class of synthetic 2D materials.

■ ASSOCIATED CONTENT

Supporting Information

The Supporting Information is available free of charge on the ACS Publications website at DOI: 10.1021/acs.nanolett.7b05178.

Additional experimental details (PDF)

■ AUTHOR INFORMATION

Corresponding Author

*E-mail: bedzyk@northwestern.edu.

ORCID

Andrew J. Mannix: 0000-0003-4788-1506

Mark C. Hersam: 0000-0003-4120-1426

Michael J. Bedzyk: 0000-0002-1026-4558

Author Contributions

#G.P.C. and A.J.M. contributed equally.

Funding

This work was supported by the National Science Foundation Materials Research Science and Engineering Center (NSF DMR-1720139) and the Office of Naval Research (ONR N00014-17-1-2993). This work was performed, in part, at the Center for Nanoscale Materials, a U.S. Department of Energy Office of Science User Facility, and supported by the U.S. Department of Energy, Office of Science, under contract no. DE-AC02-06CH11357. A.J.M. further acknowledges the National Science Foundation Graduate Fellowship Program (DGE-1324585). We thank Diamond Light Source for access to beamline I09 (proposal number SI15748) that contributed to the results presented here. We thank Dave McCue and Pardeep Khakur for assistance with our beamtime. We thank Jörg Zegenhagen for helpful discussion, Brandon Fisher for technical assistance, and Boris Yakobson for providing atomic coordinates from DFT results.

Notes

The authors declare no competing financial interest.

■ REFERENCES

(1) Ogitsu, T.; Schwegler, E.; Galli, G. Beta-rhombohedral boron: At the crossroads of the chemistry of boron and the physics of frustration. *Chem. Rev.* **2013**, *113* (5), 3425−3449.

(2) Sergeeva, A. P.; Popov, I. A.; Piazza, Z. A.; Li, W. L.; Romanescu, C.; Wang, L. S.; Boldyrev, A. I. Understanding boron through size-selected clusters: Structure, chemical bonding, and fluxionality. *Acc. Chem. Res.* **2014**, *47* (4), 1349−1358.

(3) Mannix, A. J.; Zhou, X. F.; Kiraly, B.; Wood, J. D.; Alducin, D.; Myers, B. D.; Liu, X.; Fisher, B. L.; Santiago, U.; Guest, J. R.; Yacaman, M. J.; Ponce, A.; Oganov, A. R.; Hersam, M. C.; Guisinger, N. P. Synthesis of borophenes: Anisotropic, two-dimensional boron polymorphs. *Science* **2015**, *350* (6267), 1513−1516.

(4) Feng, B.; Zhang, J.; Zhong, Q.; Li, W.; Li, S.; Li, H.; Cheng, P.; Meng, S.; Chen, L.; Wu, K. Experimental realization of two-dimensional boron sheets. *Nat. Chem.* **2016**, *8* (6), 563−568.

(5) Novoselov, K. S.; Jiang, D.; Schedin, F.; Booth, T. J.; Khotkevich, V. V.; Morozov, S. V.; Geim, A. K. Two-dimensional atomic crystals. *Proc. Natl. Acad. Sci. U. S. A.* **2005**, *102* (30), 10451−10453.

(6) Geim, A. K.; Novoselov, K. S. The rise of graphene. *Nat. Mater.* **2007**, *6* (3), 183−191.

(7) Wang, Q. H.; Kalantar-Zadeh, K.; Kis, A.; Coleman, J. N.; Strano, M. S. Electronics and optoelectronics of two-dimensional transition metal dichalcogenides. *Nat. Nanotechnol.* **2012**, *7* (11), 699−712.

(8) Ling, X.; Wang, H.; Huang, S.; Xia, F.; Dresselhaus, M. S. The renaissance of black phosphorus. *Proc. Natl. Acad. Sci. U. S. A.* **2015**, *112* (15), 4523−4530.

(9) Piazza, Z. A.; Hu, H. S.; Li, W. L.; Zhao, Y. F.; Li, J.; Wang, L. S. Planar hexagonal b(36) as a potential basis for extended single-atom layer boron sheets. *Nat. Commun.* **2014**, *5*, 3113.

(10) Zhang, Z.; Yang, Y.; Gao, G.; Yakobson, B. I. Two-dimensional boron monolayers mediated by metal substrates. *Angew. Chem., Int. Ed.* **2015**, *54* (44), 13022−13026.

(11) Boustani, I. Systematic ab initio investigation of bare boron clusters:Mdetermination of the geometryand electronic structures ofbn(n = 2−14). *Phys. Rev. B: Condens. Matter Mater. Phys.* **1997**, *55* (24), 16426−16438.

(12) Tang, H.; Ismail-Beigi, S. Novel precursors for boron nanotubes: The competition of two-center and three-center bonding in boron sheets. *Phys. Rev. Lett.* **2007**, *99* (11), 115501.

(13) Penev, E. S.; Bhowmick, S.; Sadrzadeh, A.; Yakobson, B. I. Polymorphism of two-dimensional boron. *Nano Lett.* **2012**, *12* (5), 2441−2445.

(14) Wu, X.; Dai, J.; Zhao, Y.; Zhuo, Z.; Yang, J.; Zeng, X. C. Two-dimensional boron monolayer sheets. *ACS Nano* **2012**, *6* (8), 7443−7453.

(15) Zhang, Z.; Penev, E. S.; Yakobson, B. I. Two-dimensional materials: Polyphony in b flat. *Nat. Chem.* **2016**, *8* (6), 525−527.

(16) Busse, C.; Lazic, P.; Djemour, R.; Coraux, J.; Gerber, T.; Atodiresei, N.; Caciuc, V.; Brako, R.; N'Diaye, A. T.; Blugel, S.; Zegenhagen, J.; Michely, T. Graphene on ir(111): Physisorption with chemical modulation. *Phys. Rev. Lett.* **2011**, *107* (3), 036101.

(17) Bianchini, F.; Patera, L. L.; Peressi, M.; Africh, C.; Comelli, G. Atomic scale identification of coexisting graphene structures on ni(111). *J. Phys. Chem. Lett.* **2014**, *5* (3), 467−473.

(18) Martoccia, D.; Björck, M.; Schlepütz, C. M.; Brugger, T.; Pauli, S. A.; Patterson, B. D.; Greber, T.; Willmott, P. R. Graphene on ru(0001): A corrugated and chiral structure. *New J. Phys.* **2010**, *12* (4), 043028.

(19) Farwick Zum Hagen, F. H.; Zimmermann, D. M.; Silva, C. C.; Schlueter, C.; Atodiresei, N.; Jolie, W.; Martinez-Galera, A. J.; Dombrowski, D.; Schroder, U. A.; Will, M.; Lazic, P.; Caciuc, V.; Blugel, S.; Lee, T. L.; Michely, T.; Busse, C. Structure and growth of hexagonal boron nitride on ir(111). *ACS Nano* **2016**, *10* (12), 11012−11026.

(20) Berner, S.; Corso, M.; Widmer, R.; Groening, O.; Laskowski, R.; Blaha, P.; Schwarz, K.; Goriachko, A.; Over, H.; Gsell, S.; Schreck, M.; Sachdev, H.; Greber, T.; Osterwalder, J. Boron nitride nanomesh: Functionality from a corrugated monolayer. *Angew. Chem., Int. Ed.* **2007**, *46* (27), 5115−5119.

(21) Woodruff, D. P. Surface structure determination using x-ray standing waves. *Rep. Prog. Phys.* **2005**, *68* (4), 743−798.

(22) Zegenhagen, J. Surface structure determination with x-ray standing waves. *Surf. Sci. Rep.* **1993**, *18* (7−8), 202−271.

DOI: 10.1021/acs.nanolett.7b05178
Nano Lett. 2018, 18, 2816−2821

(23) Zhang, Z.; Mannix, A. J.; Hu, Z.; Kiraly, B.; Guisinger, N. P.; Hersam, M. C.; Yakobson, B. I. Substrate-induced nanoscale undulations of borophene on silver. *Nano Lett.* **2016**, *16* (10), 6622−6627.
(24) Mannix, A. J.; Kiraly, B.; Hersam, M. C.; Guisinger, N. P. Synthesis and chemistry of elemental 2D materials. *Nat. Rev. Chem.* **2017**, *1* (2), 0014.
(25) Feng, B.; Sugino, O.; Liu, R. Y.; Zhang, J.; Yukawa, R.; Kawamura, M.; Iimori, T.; Kim, H.; Hasegawa, Y.; Li, H.; Chen, L.; Wu, K.; Kumigashira, H.; Komori, F.; Chiang, T. C.; Meng, S.; Matsuda, I. Dirac fermions in borophene. *Phys. Rev. Lett.* **2017**, *118* (9), 096401.
(26) Schwarz, M.; Riss, A.; Garnica, M.; Ducke, J.; Deimel, P. S.; Duncan, D. A.; Thakur, P. K.; Lee, T. L.; Seitsonen, A. P.; Barth, J. V.; Allegretti, F.; Auwarter, W. Corrugation in the weakly interacting hexagonal-bn/cu(111) system: Structure determination by combining noncontact atomic force microscopy and x-ray standing waves. *ACS Nano* **2017**, *11* (9), 9151−9161.
(27) Emery, J. D.; Detlefs, B.; Karmel, H. J.; Nyakiti, L. O.; Gaskill, D. K.; Hersam, M. C.; Zegenhagen, J.; Bedzyk, M. J. Chemically resolved interface structure of epitaxial graphene on SiC(0001). *Phys. Rev. Lett.* **2013**, *111* (21), 215501.
(28) Kawahara, K.; Shirasawa, T.; Arafune, R.; Lin, C. L.; Takahashi, T.; Kawai, M.; Takagi, N. Determination of atomic positions in silicene on ag(111) by low-energy electron diffraction. *Surf. Sci.* **2014**, *623*, 25−28.
(29) Borca, B.; Barja, S.; Garnica, M.; Sanchez-Portal, D.; Silkin, V. M.; Chulkov, E. V.; Hermanns, C. F.; Hinarejos, J. J.; Vazquez de Parga, A. L.; Arnau, A.; Echenique, P. M.; Miranda, R. Potential energy landscape for hot electrons in periodically nanostructured graphene. *Phys. Rev. Lett.* **2010**, *105* (3), 036804.
(30) Garcia-Lekue, A.; Balashov, T.; Olle, M.; Ceballos, G.; Arnau, A.; Gambardella, P.; Sanchez-Portal, D.; Mugarza, A. Spin-dependent electron scattering at graphene edges on ni(111). *Phys. Rev. Lett.* **2014**, *112* (6), 066802.
(31) Susi, T.; Kaukonen, M.; Havu, P.; Ljungberg, M. P.; Ayala, P.; Kauppinen, E. I. Core level binding energies of functionalized and defective graphene. *Beilstein J. Nanotechnol.* **2014**, *5*, 121−132.
(32) Plummer, E. W.; Eberhardt, W. Angle-resolved photoemission as a tool for the study of surfaces. *Adv. Chem. Phys.* **2007**, *49*, 533−656.
(33) Berman, L. E.; Bedzyk, M. J. Angular distribution of the photoelectron yield excited by two coherently coupled photon beams. *Phys. Rev. Lett.* **1989**, *63* (11), 1172−1175.
(34) Bedzyk, M. J.; Shen, Q.; Keeffe, M. E.; Navrotski, G.; Berman, L. E. X-ray standing wave study of iodine on ge(111). *Surf. Sci.* **1989**, *220* (2−3), 419−427.
(35) Golovchenko, J. A.; Patel, J. R.; Kaplan, D. R.; Cowan, P. L.; Bedzyk, M. J. Solution to the surface registration problem using x-ray standing waves. *Phys. Rev. Lett.* **1982**, *49* (8), 560−563.
(36) Laskowski, R.; Blaha, P.; Schwarz, K. Bonding of hexagonal BN to transition metal surfaces: An ab initio density-functional theory study. *Phys. Rev. B: Condens. Matter Mater. Phys.* **2008**, *78* (4), 045409.
(37) Feng, B.; Zhang, J.; Liu, R.-Y.; Iimori, T.; Lian, C.; Li, H.; Chen, L.; Wu, K.; Meng, S.; Komori, F.; Matsuda, I. Direct evidence of metallic bands in a monolayer boron sheet. *Phys. Rev. B: Condens. Matter Mater. Phys.* **2016**, *94* (4), 041408.
(38) Feng, B.; Zhang, J.; Ito, S.; Arita, M.; Cheng, C.; Chen, L.; Wu, K.; Komori, F.; Sugino, O.; Miyamoto, K.; Okuda, T.; Meng, S.; Matsuda, I. Discovery of 2d anisotropic dirac cones. *Adv. Mater.* **2018**, *30* (2), 1704025.
(39) Penev, E. S.; Kutana, A.; Yakobson, B. I. Can two-dimensional boron superconduct? *Nano Lett.* **2016**, *16* (4), 2522−2526.

DOI: 10.1021/acs.nanolett.7b05178
Nano Lett. 2018, 18, 2816−2821